J. Fluid Mech. (1980), *vol.* 99, *part* 2, *pp.* 343–364
Printed in Great Britain

Numerical analysis of the nonlinear propagation of plane periodic waves in a relaxing gas

By I. S. SOUTHERN† AND N. H. JOHANNESEN
Department of the Mechanics of Fluids, University of Manchester, England

(Received 31 July 1979 and in revised form 28 November 1979)

The waves propagating from an oscillating plane piston into a vibrationally relaxing gas are calculated by an exact numerical method ignoring viscosity and heat conduction. Secondary effects due to the starting of the piston from rest and to acoustic streaming can be eliminated from the calculated flows, leaving a truly periodic progressive wave which can be analysed and compared with approximate solutions. It is found that for moderate amplitude waves nonlinearity is only important as a convective effect which produces higher harmonics, whereas dissipation is adequately described by linear theory.

1. Introduction

In several earlier papers members of our department have studied nonlinear wave propagation in a vibrationally relaxing gas by numerical integration of the exact equations ignoring viscosity and heat conduction. The translational and rotational modes are assumed to move through equilibrium states and the only dissipative mechanism outside shock waves is the non-equilibrium production of entropy due to the lag in the vibrational mode. Hornby & Johannesen (1975) and Kao & Hodgson (1978) considered steady wedge and cone flows, respectively, while Dain & Hodgson (1975) treated the unsteady flow due to an impulsively started piston. The numerical calculations were carried out for a pure gas with large vibrational specific heat, but Hodgson & Johannesen (1976) demonstrated that the calculations could be used to obtain tentative results relevant to air which has two vibrational modes, both with very small vibrational specific heats at meteorological temperatures, but with vastly different, strongly humidity-dependent, relaxation times.

In this paper we report on the first stage of a research programme stimulated by the current interest in possible nonlinear effects in aircraft-noise propagation, as discussed by Pernet & Payne (1971) and by Webster & Blackstock (1978). These are essentially long-distance accumulative effects of locally minute departures from linear behaviour which are always present in wave propagation. It is only the fact that waves decay due to dissipation and spherical spreading that makes them unimportant in most practical cases. No precise criterion exists at the moment for predicting if and when they are significant in practice.

The work completed so far concerns the wave pattern produced in a gas by a sinusoidally oscillating piston, but work is in progress on the practically more

† Present address: Rolls-Royce Ltd, Aero Division, Derby, England.

0022–1120/80/4486–1510 $02.00

important pulsating-sphere problem. Extensions to more complicated oscillations and to gases with more than one vibrational mode seem entirely possible. Even the 'simple' piston case was found to have features not generally discussed in the available literature on nonlinear acoustics. Of particular interest are the starting and streaming effects which can, however, be separated out so that the truly periodic part of the wave can be analysed. The wave form is found to display both steepening and skewness.

The results throw some light on the relative importance of convection and dissipation, and it is found that in the flows calculated the latter can always be described by linear theory. This adds support to methods which combine nonlinear convection effects with linear dissipation such as the one proposed by Pernet & Payne (1971) in which the Fubini solution is combined with linear dissipation.

The vibrational specific heat in all our examples is large. This ensures large rates of amplitude decay and the absence of shocks except perhaps in the very far field. Our comparison of exact calculations with approximate results using the Pernet & Payne method does not therefore truly assess its applicability to air, although we present some suggestions that it may be improved by including higher-order terms in the expansion of the Bessel function appearing in the Fubini solution. The high values of the vibrational specific heat lead to large differences between the frozen and equilibrium sound speeds and therefore to large variations in the frequency-dependent linearized (Kneser) speed of sound, so that the exact linear expressions have to be used.

We first outline the basic theory and calculation method and then present in turn the isentropic flow results and their approximation, and the linear theory of dissipation and attenuation. A brief discussion of starting and streaming effects is followed by some typical examples of wave-profile development, and we conclude with examples of Fourier analysis of the results and comparison with the Pernet & Payne method.

2. Basic theory and calculation method

The basic equations and formulation of their characteristics are exactly the same as those used by Dain & Hodgson (1975). The relaxation equation is

$$D\sigma/Dt = \rho\Phi(\bar{\sigma}-\sigma) = (\bar{\sigma}-\sigma)/\tau, \tag{1}$$

where σ is the vibrational energy and $\bar{\sigma}$ its local equilibrium value, t the time, and ρ the density. The quantity $\rho\Phi$ is the relaxation frequency and τ the relaxation time; Φ depends on temperature only, but in all numerical calculations Φ was assumed to be constant in any one flow. Similarly the vibrational specific heat cR (where R is the specific gas constant) was assumed to be constant within any one flow.

The three families of characteristics are:

(i) the right-hand characteristics

$$dx/dt = u+a \tag{2a}$$

on which

$$dp+\rho a\,du = -(\gamma-1)\rho^2\Phi(\bar{\sigma}-\sigma)dt; \tag{2b}$$

(ii) the left-hand characteristics

$$dx/dt = u-a \tag{3a}$$

on which

$$dp-\rho a\,du = -(\gamma-1)\rho^2\Phi(\bar{\sigma}-\sigma)dt; \tag{3b}$$

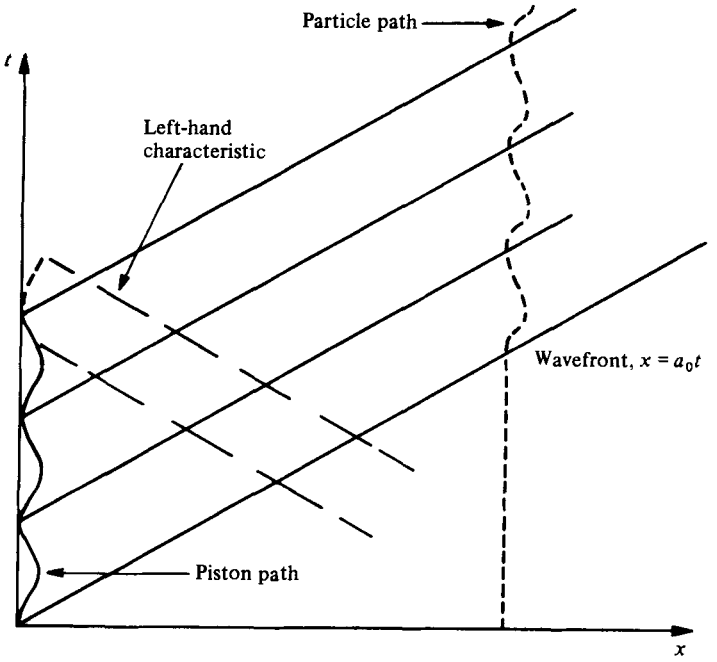

FIGURE 1. The three families of characteristics: x, t diagram.

(iii) the particle paths

$$dx/dt = u \tag{4a}$$

on which

$$dp - a^2 d\rho = -(\gamma - 1)\rho^2 \Phi(\bar{\sigma} - \sigma)dt. \tag{4b}$$

Here x is the distance measured from the rest position of the piston, u the velocity magnitude, and a the frozen speed of sound; p is the pressure and γ the frozen specific heat ratio.

The three families are shown for the piston problem on figure 1. If the piston starts moving at $t = 0$ the wave front is $x = a_0 t$, where suffix 0 indicates rest conditions ahead of the wave field. The retarded time co-ordinate is $y = t - x_0/a_0$, where x_0 is the initial (rest) value of x on a particle path.

The boundary conditions for all the flows calculated are of the form

$$\left.\begin{aligned} x_P &= 0 \quad \text{for} \quad t < 0, \\ x_P &= f(t) \quad \text{for} \quad t \geqslant 0, \end{aligned}\right\} \tag{5}$$

where suffix P refers to the piston and $f(t)$ is of a form which gives a harmonic oscillation of the piston. Typical boundary conditions used were

$$x_P = \frac{u_1}{\omega}(1 - \cos \omega t) \tag{6}$$

and

$$x_P = -\frac{u_1}{\omega} \sin \omega t, \tag{7}$$

where u_1 is the velocity amplitude on the piston and ω the radian frequency. The second boundary condition gives zero mean displacement of the piston.

The flows are governed by three parameters: $u_1/a_0 = \epsilon$ which is always a small parameter, c which is never more than $O(1)$, and $\omega\tau$ which may cover the whole range from very small to very large values.

Excellent surveys of nonlinear acoustic theories have been given by Blackstock (1962) and by Rudenko & Soluyan (1977). Blythe (1969) gave a survey of the theories of general nonlinear, non-equilibrium flows and pointed out that second-order theories can be developed not only by ignoring terms of order ϵ^3 but also by ignoring terms of order $\epsilon^2 c$ in the small energy limit, and by ignoring terms of order $\epsilon^2\omega\tau$ and $\epsilon^2/\omega\tau$ in the low- and high-frequency limits, respectively.

The low-frequency flows are governed by Burgers's equation and have been discussed extensively in the literature. High-frequency flows are, although amenable to approximate theoretical analysis, not of particular practical importance, because the neglect of heat conduction and viscosity (and of rotational relaxation) becomes progressively less realistic as the frequency increases. We shall therefore concentrate on numerical calculation of flows for which $\omega\tau$ is of order unity, although reference will be made to both low- and high-frequency flows.

The numerical solutions were obtained by the usual step-by-step method and will be presented as values of the variables plotted as functions of the retarded co-ordinate y on particle paths. As the amplitude of the oscillations of a particle path is very small the curves thus obtained correspond very closely, in the case of the pressure, to the signal that would be received by a microphone positioned at the particular value of x_0. It is not possible to give a precise analysis of the accuracy of the numerical results, but numerous checks, including variation of step size and determination of shock formation distance, were all satisfactory. The fact that the very low amplitude far field turns out to be periodic (repeating) in time is also a strong indication of correctness. The amplitude decay rate agreed to four figures with the linear decay rate. In earlier papers using the same approach we found excellent agreement with the known exact far-field solution.

We shall retain the dimensional forms of the variables in most equations but the calculated results will be presented in non-dimensional form according to the following set of equations in which $\hat{}$ denotes non-dimensional quantities:

$$\hat{p} = p/p_0, \quad \hat{u} = u(RT_0)^{-\frac{1}{2}}, \tag{8), (9}$$

$$(\hat{x}, \hat{\alpha}^{-1}) = (x, \alpha^{-1})\rho_0\Phi(RT_0)^{-\frac{1}{2}}, \tag{10}$$

$$(\hat{t}, \hat{y}, \hat{\omega}^{-1}) = (t, y, \omega^{-1})\rho_0\Phi; \tag{11}$$

α is the linear attenuation rate introduced in §4, and T_0 is the 'rest' gas temperature.

3. Isentropic theory and the Fubini approximation

In the absence of relaxation the equations of §2 simplify to the standard equations of one-dimensional unsteady, isentropic flow. These cover not only the case of $c = 0$ but also the limiting cases of frozen and equilibrium flow. They are of course well known, and exact solutions exist for the sinusoidally oscillating piston. It should, however, be emphasized that the term 'sinusoidal' is not precise in the context of the exact equations: it must be specified which variable is sinusoidal. In our numerical

calculations this will always be the velocity on the piston path, i.e. at $x_0 = 0$ rather than at $x = 0$.

The solutions of the exact equations or numerical integration of them in characteristic form for the boundary condition (6), showed the familiar steepening of the wave profile as the wave propagates, with a shock forming at the wave front at the shock formation distance (e.g., see Johannesen & Scott 1978)

$$x_s = 2a_0^2/(\gamma+1)u_1\omega, \tag{12}$$

i.e. at the time

$$t_s = \frac{2a_0}{(\gamma+1)u_1\omega}. \tag{13}$$

We are only concerned with that part of the flow which lies between the piston and the left-hand characteristic through (x_s, t_s).

If we use the characteristic form of the equations and the relation $dx/dt = u$ on a particle path, a parametric representation of the particle path can be obtained for the boundary condition (6). The analysis is straightforward and will not be given. The result is

$$t = \frac{x_0}{a_0}\left[1 + \frac{(\gamma-1)u_1}{2a_0}\sin\omega t_P\right]^{(1+\gamma)/(1-\gamma)} + t_P, \tag{14}$$

$$x = \frac{x_0}{a_0}\left[a_0 + \frac{(\gamma+1)u_1}{2}\sin\omega t_P\right]\left[1 + \frac{(\gamma-1)u_1}{2a_0}\sin\omega t_P\right]^{(1+\gamma)/(1-\gamma)} + \frac{u_1}{\omega}(1-\cos\omega t_P), \tag{15}$$

$$u = u_1 \sin\omega t_P, \tag{16}$$

where x is x_0 if t_P is zero.

The following implicit solution for u along a particle path is then easily obtained,

$$\frac{u}{u_1} = \sin\omega\left[t - \frac{x_0}{a_0}\left(1 + \frac{(\gamma-1)u}{2a_0}\right)^{(1+\gamma)/(1-\gamma)}\right]. \tag{17}$$

Various forms of approximate solutions exist; the best known of these is probably the one due to Fubini. In general such solutions must be equivalent to a solution of the following approximations to (14), (15) and (16),

$$t = \frac{x_0}{a_0}\left[1 - \frac{(\gamma+1)u_1}{2a_0}\sin\omega t_P\right] + t_P, \tag{18}$$

$$x = x_0 + \frac{u_1}{\omega}(1-\cos\omega t_P), \tag{19}$$

$$u = u_1 \sin\omega t_P, \tag{20}$$

or of the following approximations to equation (17),

$$\frac{u}{u_1} = \sin\omega\left[t - \frac{x_0}{a_0}\left(1 - \frac{(\gamma+1)u}{2a_0}\right)\right] + O(\epsilon^2) \tag{21a}$$

$$= \sin\omega\left(t - \frac{x_0}{a_0}\right) + \frac{x_0}{2x_s}\sin 2\omega\left(t - \frac{x_0}{a_0}\right) + O(\epsilon^2). \tag{21b}$$

An alternative to the description of the changing wave form as being due to steepening, is to examine the growth of higher harmonics. This will be done in §8 by Fourier analysing the wave forms. Here we shall discuss the approximate isentropic Fubini solution, which will later be combined with linear attenuation theory, and not present the results of the exact numerical calculations for isentropic flow except to mention the tendency for the nth harmonic to grow as x^{n-1} in the near field, i.e. for $x_0 \ll x_s$.

The Fubini solution is obtained from the implicit solution (21*a*). As shown by Blackstock (1962) and by Rudenko & Soluyan (1977), an approximate explicit solution may be obtained by Fourier analysing this equation. The Fourier coefficients thus obtained are in terms of integrals of the type used by Bessel to define his function. The following solution is then obtained,

$$\frac{u}{u_1} = \sum_{n=1}^{\infty} \frac{2x_s}{nx_0} J_n\left(\frac{nx_0}{x_s}\right) \sin n\omega y + O(\epsilon^2) \tag{22}$$

and is usually attributed to Fubini. Also, if n is an integer,

$$J_n(x) = \sum_{r=0}^{\infty} \frac{(-1)^r}{r!(n+r)!} \left(\frac{x}{2}\right)^{n+2r}, \tag{23}$$

so that, if $\bar{u}_n$ is the amplitude of the nth velocity harmonic,

$$\begin{aligned} \frac{\bar{u}_n}{u_1} &= \sum_{r=0}^{\infty} \frac{(-1)^r}{r!(n+r)!} \left(\frac{nx}{2x_s}\right)^{n+2r-1} \\ &= \frac{1}{n!}\left(\frac{nx}{2x_s}\right)^{n-1} + O(\epsilon^{n+1}) \end{aligned} \tag{24}$$

for $x \ll x_s$.

Thus, although equation (22) is not really accurate to more than order ϵ it appears to explain the behaviour of the higher harmonics already mentioned. Hence, even though

$$\bar{u}_n/u_1 = O(\epsilon^{n-1})$$

the Fubini solution predicts that

$$\bar{u}_n \propto x^{n-1}$$

in the near field. Nevertheless, it must be stressed that the accuracy with which (22) describes the behaviour of the third and higher harmonics is so far unknown. Some measure of its effectiveness can however be obtained from the following analysis in terms of the boundary condition

$$u = u_1 \sin \omega t_P \quad \text{on} \quad x_P = 0. \tag{25}$$

This problem is analogous to the oscillating piston problem, since the Fubini solution applies to both cases to order ϵ^2 on lines of constant x and x_0, respectively. Hence for equation (25) a general right-hand characteristic has the form

$$x = \left(a_0 + \frac{\gamma+1}{2} u_1 \sin \omega t_P\right)(t - t_P) \tag{26}$$

on which

$$u = u_1 \sin \omega t_P.$$

Eliminating t_P then gives the implicit solution

$$u = u_1 \sin\omega\left[t - \frac{x_0}{a_0 + \frac{1}{2}(\gamma+1)u}\right] \tag{27}$$

on lines of constant x, and this agrees with (21a) to order ϵ. However, the flow with equation (25) as the boundary condition can also be determined by solving the exact equation for isentropic flow (see Blackstock 1962)

$$\frac{\partial u}{\partial X} = \frac{\gamma+1}{2a_0^2} u\left(\frac{\partial u}{\partial Y} - a_0 \frac{\partial u}{\partial X}\right), \tag{28}$$

where $X = x$ and $Y = t - x/a_0$, which to order ϵ^2 becomes

$$\frac{\partial u}{\partial X} = \frac{\gamma+1}{2a_0^2} u \frac{\partial u}{\partial Y}. \tag{29}$$

Both this equation which has the solution (21a) and equation (28) which has the solution (27) can therefore be solved by iteration, since the right-hand sides are small.

The iterative solution of both the equations will be briefly discussed in the rest of this section, for two main reasons. Firstly, both solutions provide an interesting model of how higher harmonics are produced in a wave as it propagates. Secondly, because the agreement between the Fubini solution and the numerical Fourier analysis results, in describing the behaviour of the higher harmonics, requires some explanation, particularly since the growth of higher harmonics in a wave in a gas with vibrational relaxation are described by using an approximation which employs the Fubini solution, in §5. However, it must be stressed that the analysis which will be given is not supposed to be a rigorous or full discussion of the problem. That would be a major task. Our concern is simply with providing explanations of phenomena for which precise descriptions do not appear to exist in the literature. A rigorous iterative solution of the oscillating piston problem is given by Blackstock (1962), but the following much simpler model will be sufficient for our purpose.

Firstly consider equation (29). If the right-hand side is ignored as being small, this has the solution

$$u = u_1 \sin\omega Y. \tag{30}$$

Substituting this solution in the right-hand side of equation (29) then gives

$$\frac{\partial u}{\partial X} = \frac{u_1}{2x_s} \sin 2\omega Y$$

and this has the solution

$$u = u_1 \sin\omega Y + \frac{u_1 X}{2x_s} \sin 2\omega Y. \tag{31}$$

Similarly the next iteration gives

$$u = u_1 \sin\omega Y\left(1 - \frac{X^2}{8x_s^2}\right) + \frac{u_1 X}{2x_s} \sin 2\omega Y + 3\frac{u_1 X^2}{8x_s^2} \sin 3\omega Y + \frac{u_1 X^3}{12x_s^3} \sin 4\omega Y \tag{32}$$

and so on.

In fact, with each iteration more and more terms in the Fubini solution will be generated. Thus the terms in the first three harmonics in (32) are the leading terms in these harmonics in the Fubini solution. The term in the fourth harmonic is only part of the leading term in the Fubini solution. The rest of this is produced in the next

iteration from the first and third harmonics. Hence, the nonlinear term in (29) will always lead to the nth harmonic producing $2n$th harmonics from itself, and to the nth and mth harmonics producing $(n+m)$th and $(n-m)$th harmonics. What is more, the terms in the solution will always be in $\sin(n\omega Y)$ since the Fubini solution is symmetric.

The iterative solution of (28) will obviously be more complicated than that of (29). However, three iterations can be done quite easily. The first has the solution given by (30), the second the solution given by (31) and the third the solution

$$u = \left(1 - \frac{X^2}{8x_s^2}\right) u_1 \sin\omega Y - \frac{a_0 u_1 X}{4x_s^2\omega}\cos\omega Y + \frac{u_1 X}{2x_s}\sin 2\omega Y$$
$$+ \frac{3u_1 X^2}{8x_s^2}\sin 3\omega Y + \frac{a_0 u_1 X}{4x_s^2\omega}\cos 3\omega Y + \frac{u_1 X^3}{12x_s^3}\sin 4\omega Y + \frac{a_0 u_1 X^2}{16x_s^3\omega}\cos 4\omega Y - \frac{a_0 u_1 X^2}{16x_s^3\omega}. \tag{33}$$

Thus, the extra term in (28) produces cosine terms in the solution, which lead to an asymmetric wave, as well as sine terms, and terms which make the mean of the wave x dependent. However, the terms affecting the mean of the wave are due to our examining the wave on lines of constant x, rather than on particle paths in the flow. No such effect occurs in the oscillating piston problem. Nevertheless, their appearance does highlight the difficulty in applying exact results, for the boundary condition given by (25), to the oscillating piston problem.

The solution given by (33) is in fact sufficiently informative for the effect of the extra term in (28) to be described simply from (33) and (32). Thus it can be seen that the effects of the cosine terms in (33) will be small if

$$a_0/\omega X \ll 1.$$

This will always be the case, since in the right-hand side of (28)

$$\frac{\partial}{\partial Y} \sim \omega, \quad a_0\frac{\partial}{\partial X} \sim \frac{a_0}{X},$$

so that

$$\frac{\partial}{\partial Y}\Big/ a_0\frac{\partial}{\partial X} \sim \frac{\omega X}{a_0} \gg 1.$$

Thus, the extra term in (28) will only effect the leading term for each harmonic in the Fubini solution as long as X is much smaller that a_0/ω which is much smaller than x_s.

Finally, in linear acoustics the intensity of a wave is proportional to its amplitude squared. Thus, the intensity of any harmonic in a wave will be roughly proportional to $\bar{u}_n^2$. Hence, if in a simple model ten per cent of the intensity of a pure tone is fed into a second harmonic, $\bar{u}_1$ will only decrease by approximately five per cent. However, $\bar{u}_2$ will grow from nothing to roughly thirty per cent of the original pure tone amplitude. This demonstrates how little $\bar{u}_1$ need to attenuate for significant levels of high harmonics to be present in a wave.

The results given in this section will be used for comparison with similar results in a gas with vibrational relaxation. In particular, the discussion of the applicability of

the Fubini solution in determining the near field growth of harmonics will be of use in §§ 5 and 8. These discuss the approximate method, already mentioned in this section, which uses the Fubini solution to determine wave propagation in a gas with vibrational relaxation.

4. Linearized dissipation theory

The linearized theory of sound absorption in a relaxing gas is well known, and in most cases further simplifications are introduced after linearization. For the large values of c used in the present work it is, however, necessary to use the full linearized expressions for the frequency-dependent absorption rate and speed of sound. These were probably first given by Herzfeld & Litovitz (1959), but we shall quote the expressions without derivation from the recent survey article by Johannesen & Hodgson (1979). With their definition of the linear amplitude absorption rate α_L and the linear speed of sound a_L, we have

$$\alpha_L = \omega B/a_e, \quad a_L = Aa_e, \tag{34), (35}$$

where we shall in this section for clarity use the suffixes e and f to indicate equilibrium (low-frequency) and frozen (high-frequency) values. Here B and A are defined by

$$B = \frac{\Omega Q A}{2(1+\Omega^2)}, \tag{36}$$

$$A^2 = \frac{2(1+\Omega^2)}{\Omega^2 Q^2}\{([1+(1-Q)\,\Omega^2]^2+\Omega^2 Q^2)^{\frac{1}{2}}-(1+(1-Q)\,\Omega^2)\}, \tag{37}$$

where

$$\Omega = \omega\tau c_{pf}/c_{pe} \tag{38}$$

and

$$Q = R^2 c/c_{ve}c_{pf}. \tag{39}$$

The high-frequency limits are

$$A_f = (\gamma_f/\gamma_e)^{\frac{1}{2}} \tag{40}$$

and

$$\alpha_f = \frac{(\gamma_f-1)^2 c}{2\gamma_f \tau a_f}; \tag{41}$$

and the low-frequency limits are

$$A_e = 1, \tag{42}$$

$$B_e = \frac{\Omega Q}{2(1+\Omega^2)} = \frac{\omega\tau R^2 c}{2c_{pe}c_{ve}}, \tag{43}$$

$$\alpha_e = \frac{\omega^2\tau R^2 c}{2a_e c_{pe}c_{ve}} = \mu_v \frac{\omega^2}{2\rho a_e^3}, \tag{44}$$

where μ_v is the bulk viscosity.

The 'exact' linearized values of attenuation rate and speed of sound will be used in the discussion of the numerically calculated results in later sections.

5. The Pernet & Payne method

This method was originally devised to model nonlinear wave propagation in a tube filled with gas with a known decay rate due to wall friction. Pernet & Payne then went on to apply the technique to wave propagation in the atmosphere, and, in fact, it can in principle be applied to all wave propagation which satisfies the following two conditions: firstly, an analytic model must exist for the growth of harmonics in the equivalent isentropic flow and, secondly, the linear decay rate for the particular type of wave and attenuation mechanism must be known. These conditions are necessary because the method basically assumes that at any point in the flow harmonic growth depends on the amplitude of the fundamental, and is as in isentropic flow, and that dissipation is a linear process.

Our description of the method differs from Pernet & Payne's in certain respects. They consider pressure, but our description is in terms of velocity. Also, their model appears to be somewhat inconsistent with a version of the Fubini solution suited to initial-value problems being used in a boundary-value problem, whereas our model is consistent in this respect. There is also a physical difficulty in applying the method to our problem, since only one speed of sound is assumed. This is the case when either c is very small or attenuation is caused by some mechanism other than vibrational relaxation. However, in our flows with large values of c, a range of sound speed is available. We have used the frozen speed of sound since there is some indication that wave steepening is governed by the behaviour of the frozen characteristics. This is, however, a point to be remembered when the approximate results are compared with our exact numerical calculations.

The technique is easily understood by considering the second harmonic in the wave in velocity produced by the boundary condition

$$u = u_1 \sin \omega t \quad \text{at} \quad x = 0. \tag{45}$$

In isentropic flow, the rate of change of $\bar{u}_2$ can be found from the Fubini solution. Thus for small u from equation (24)

$$\frac{d\bar{u}_2}{dx} = \frac{(\gamma+1)u_1^2\omega}{4a_0^2}. \tag{46}$$

Pernet & Payne's method would appear to assume that the local rate of change of $\bar{u}_2$, due to convection in a decaying wave, is also given by this type of expression. Therefore, if the local amplitude of the fundamental in the decaying wave is $\bar{u}_1$,

$$\frac{d\bar{u}_2}{dx} = \frac{(\gamma+1)\bar{u}_1^2\omega}{4a_0^2}. \tag{47}$$

However, according to linear theory $\bar{u}_1 = u_1 \exp(-\alpha_1 x)$, where α_1 is equal to α_L, the decay rate for the fundamental in the wave. What is more, $\bar{u}_2$ will also change due to dissipation. Hence, if it is assumed that the total rate of change is due to convection (given by (47)) and dissipation (given by linear acoustics) the following equation is obtained,

$$\frac{d\bar{u}_2}{dx} + \alpha_2 \bar{u}_2 = \frac{(\gamma+1)\omega}{4a_0^2} u_1^2 \exp(-2\alpha_1 x). \tag{48}$$

This is the same type of equation as was obtained by Pernet & Payne. However, they only describe its derivation briefly and it may therefore be slightly different from ours. With $\bar{u}_2 = 0$ at $x = 0$ the solution is

$$\bar{u}_2 = \frac{u_1}{2x_s(\alpha_2 - 2\alpha_1)}[\exp(-2\alpha_1 x) - \exp(-\alpha_2 x)], \tag{49}$$

where x_s here and elsewhere in this section is the isentropic shock formation distance, and is used only to simplify the algebra.

The corresponding general equation for the nth harmonic can then be shown to be

$$\frac{d\bar{u}_n}{dx} + \alpha_n \bar{u}_n = u_1 \frac{(n-1)}{n!}\left(\frac{n}{2x_s}\right)^{n-1} x^{n-2} \exp(-n\alpha_1 x), \tag{50}$$

and Pernet & Payne point out that this equation has a general, if complicated, solution. However, we chose the more long-winded approach of solving the corresponding equations for n equals 3, 4, 5, and 6. The solutions are given in the appendix and will be compared with numerically calculated results in § 8. Also, certain general points about the method will be made later, but first ways of extending the approach will be discussed briefly. Equation (49) might be improved by taking extra terms in equation (24) to describe convective steepening effects in the second harmonic. Thus, including the term in r equals one leads to the following equation for $\bar{u}_2$,

$$\frac{d\bar{u}_2}{dx} + \alpha_2 \bar{u}_2 = \frac{u_1}{2x_s}\exp(-2a_1 x) - \frac{u_1}{2x_s^3} x^2 \exp(-4\alpha_1 x), \tag{51}$$

and this has the solution

$$\begin{aligned}\bar{u}_2 = {} & \frac{u_1}{2x_s(\alpha_2 - 2\alpha_1)}[\exp(-2\alpha_1 x) - \exp(-\alpha_2 x)] \\ & + \frac{u_1}{x_s^3(4\alpha_1 - \alpha_2)^3}[\exp(-4\alpha_1 x) - \exp(-\alpha_2 x)] \\ & + \frac{u_1}{2x_s^3(4\alpha_1 - \alpha_2)}\left(x^2 + \frac{2x}{4\alpha_1 - \alpha_2}\right)\exp(-4\alpha_1 x).\end{aligned} \tag{52}$$

A better approximation for the behaviour of the fundamental can also be found from this approach. Thus taking the terms in r equals 0 and 1 in equation (24) gives

$$\bar{u}_1 = u_1 - \frac{u_1}{2}\left(\frac{x}{2x_s}\right)^2, \tag{53}$$

so that

$$\frac{d\bar{u}_1}{dx} = -\frac{u_1 x}{4x_s^2} = -\frac{u_1^3(\gamma+1)^2\omega^2 x}{16a_0^4}. \tag{54}$$

This leads to the following equation for $\bar{u}_1$,

$$\frac{d\bar{u}_1}{dx} + \alpha_1 \bar{u}_1 = -\frac{u_1 x}{4x_s^2}\exp(-3\alpha_1 x), \tag{55}$$

which has the solution

$$\bar{u}_1 = u_1 \exp(-\alpha_1 x)\left[1 - \frac{1 - \exp(-2a_1 x)(1 + 2\alpha_1 x)}{16x_s^2\,\alpha_1^2}\right], \tag{56}$$

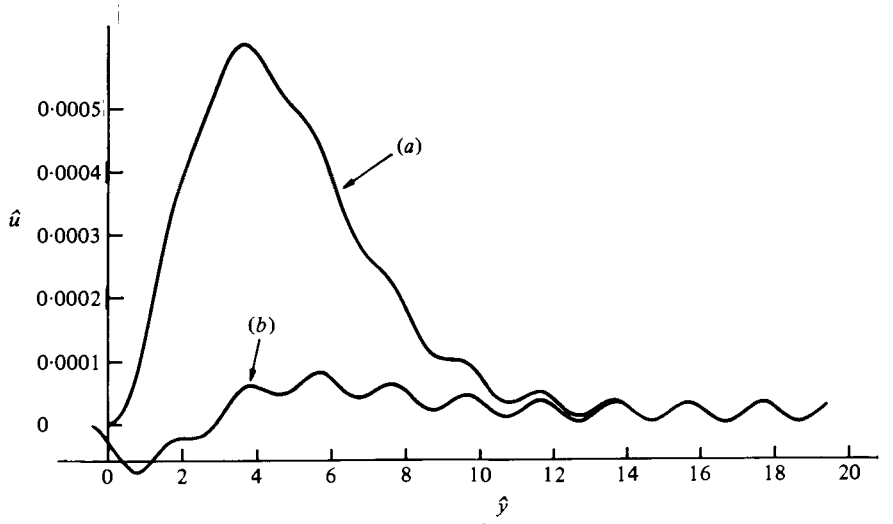

FIGURE 2. Velocity profiles on the particle path $\hat{x}_0 = 71$ for flows with $\hat{u}_1 = 0{\cdot}01$, $c = 2{\cdot}50$, and $\hat{\omega} = \pi$. The boundary conditions are: (*a*) equation (57); (*b*) equation (58).

and this gives an indication of the reduction in the amplitude of the fundamental due to feeding of the higher harmonics.

An assessment of the method applied to our problem is given in § 8 where it is also demonstrated that taking more terms in the series expansion leads to a definite improvement.

6. Starting and streaming effects

Before we can proceed to the discussion of sample numerical results for plane periodic wave propagation we must consider two secondary effects which emerged during the numerical calculations. Both effects are clearly demonstrated on figure 2 which shows velocity profiles on the particle path $\hat{x}_0 = 71$ for the two boundary conditions

$$\left.\begin{aligned} x_P &= 0 \quad \text{for} \quad t_P \leqslant 0, \\ x_P &= \frac{u_1}{\omega}(1-\cos\omega t_P) \quad \text{for} \quad t_P \geqslant 0, \end{aligned}\right\} \tag{57}$$

and

$$\left.\begin{aligned} x_P &= 0 \quad \text{for} \quad t_P \leqslant 0, \\ x_P &= -\frac{u_1}{\omega}\sin\omega t_P \quad \text{for} \quad t_P \geqslant 0, \end{aligned}\right\} \tag{58}$$

with $\hat{u}_1 = 0{\cdot}01$, $c = 2{\cdot}50$, and $\hat{\omega} = \pi$. A phase shift has been introduced in the bottom curve to make the waves coincide at large y.

The transient starting effect will not be discussed in detail. It manifests itself by the first half cycle propagating in a different manner to that of the rest of the wave. For the boundary condition (57) the dominating effect is of order ϵ and is due to the mean displacement of the piston changing to a non-zero value when it is oscillating.

The width of the starting region grows as $x^{\frac{1}{2}}$ and its amplitude decays as $x^{-\frac{1}{2}}$. This behaviour is characteristic of a single pulse in the low-frequency limit as discussed by Lighthill (1956). Indeed, if the piston was stopped after a finite time the pulse thus created would completely swallow the oscillating motion in the far field, where the pulse shape would depend only on the gross features of the piston motion and not on the oscillation. In our cases where it is the computation rather than the piston which is stopped after a finite time the starting effect will nevertheless in the case of the boundary condition (57) dominate a larger and larger part of the flow as we move away from the piston.

As already mentioned this start effect is of order ϵ and completely dominates a second starting effect of order ϵ^2. This smaller effect is related to the discontinuity in acceleration at t equals zero on the piston path, and a similar effect was observed by Blackstock (1964) in solving Burgers's equation for an oscillating piston. It can be observed on the lower curve on figure 2 corresponding to the boundary condition (58) which expands the gas initially and does not alter the mean displacement of the piston as it oscillates. It will be seen that the starting effect for the latter boundary condition is of much smaller amplitude, although the widths of the two effects seem to be roughly the same.

The results §§7 and 8 are for flows with equations (58) as the boundary condition. This was used in preference to (57) since it was thought that the steepness of the starting effect of order ϵ might lead to shock formation in the flow before shocks formed in the continuous wave profile. In fact, the general tendency appears to be for shocks to form simultaneously in either starting effect and in the continuous wave profile. However, this point has not been studied in detail. In any case, the decay in the amplitude of both starting effects was roughly as $x^{-\frac{1}{2}}$ and the growth in width as roughly $x^{\frac{1}{2}}$. This proved to be a problem in the numerical calculations, since the time for which a computer program can run is limited. Hence, since the starting effect is related to those parts of the particle paths close to the wave front which were calculated first, much of the program running time was spent calculating the starting effect.

The continuous wave profiles in figure 2 have means which differ from rest gas conditions. In fact, the mean in the wave in any variable changes in the near field, and then approaches a constant value in the far field which is not equal to the rest gas value. The variation in the mean of the velocity wave which manifests itself by there being a finite outward velocity in the far field is referred to as acoustic streaming. This effect is a direct result of entropy production on particle paths in the flow. Although this entropy production is only or order ϵ^2 and dominates only in the near field the effect spreads outward and is still of order ϵ^2 in the far field. Hence, as the amplitude of the continuous wave profile decays from order ϵ to order ϵ^2 and smaller the effect becomes more noticeable and will eventually far exceed the amplitude of the oscillations.

The various approximate nonlinear theories in general account for entropy production attenuation of the wave but ignore the entropy after it has been produced and hence miss an interesting accumulative effect in the flow.

A simple theory was developed which assumed that the entropy production leads to a monotonic increase in mean temperature on a particle path in the near field whilst the mean pressure remains roughly constant, the underlying idea being that

the pressure can relieve itself as a wave propagating outward. The result is of course a monotonic reduction in mean density in the near field, and the mass conservation law then leads to a constant mean outflow velocity in the far field. This extra flow produced by the entropy production in the near field, is in the far field similar to that produced by an impulsively started piston, and the numerically found 'streaming' quantities were found to obey the linearized shock wave relations (using the equilibrium speed of sound) which are of course identical to the linear acoustics relations. The theoretical model gave the right order of magnitude for the streaming quantities, but numerically it did not quite match the characteristics flow calculations.

7. Typical results for wave steepening and dissipation

A large number of flows with pure tone boundary conditions were calculated. Each calculation is quite time consuming and it was not considered reasonable to attempt to cover all possible values of the parameters. As already mentioned, the flows with $\omega\tau$ of order one were considered of particular interest. In this section we discuss just one of the calculated flows in order to demonstrate some of the features which emerged from the exact numerical calculations and which are not obvious from approximate theories.

Figure 3 shows the development of the pressure wave form with increasing x for a flow with $x_P = -(u_1/\omega)\sin\omega t_P$ and $\hat{u}_1 = 0{\cdot}015$, $c = 1{\cdot}00$, and $\hat{\omega} = \pi$. This particular flow was chosen because it demonstrates most of the effects with no single one dominating. The wave form steepens due to convection in the near field, continues to change in the far field due to what we shall describe as linear dispersion and decays in amplitude throughout its propagation at a rate close to that predicted by linear theory.

In addition to the steepening the wave develops considerable skewness in the near field but at $\hat{x} \sim 100$ when the amplitude has fallen to 1/100 of its original value the steep part is beginning to become localized and this steep region gradually develops into a distinct kink which travels through the wave and decays in relative amplitude. It is a remarkable feature of figure 3 that the wave has still got a distinct detailed structure which the numerical method allows us to calculate even at such large distances that the overall amplitude of the wave has decreased to less than 1/1000 of its value at $x_0 = 0$. We also note that in the last wave profile on figure 3 the streaming effect is considerably larger than the wave amplitude.

The behaviour of the kink can be explained by linear dispersion. The kink is a localized high-frequency region which therefore has a higher linear propagation speed than the rest of the wave.

The complete wave development is given on figure 4(*a*) which shows successive velocity profiles on equally spaced particle paths in the flow since the departure from straight lines of the particle paths is negligible on the scale of the figure. The wave decays with x and has virtually disappeared when $\hat{x}$ is greater than 100.

On figure 4(*b*) linear dissipation has been removed by multiplying all amplitudes by $\exp(\hat{\alpha}\hat{x}_0)$. We see that the change in overall amplitude on this figure is very small, demonstrating that the decay closely obeys linear acoustics. The figure clearly shows the starting effect. It also shows the relative movement of parts of the signal relative to the frozen characteristics ($\hat{Y} \sim$ constant). Thus in the near field the peak converges towards the frozen characteristics due to convection whereas in the far field the peak

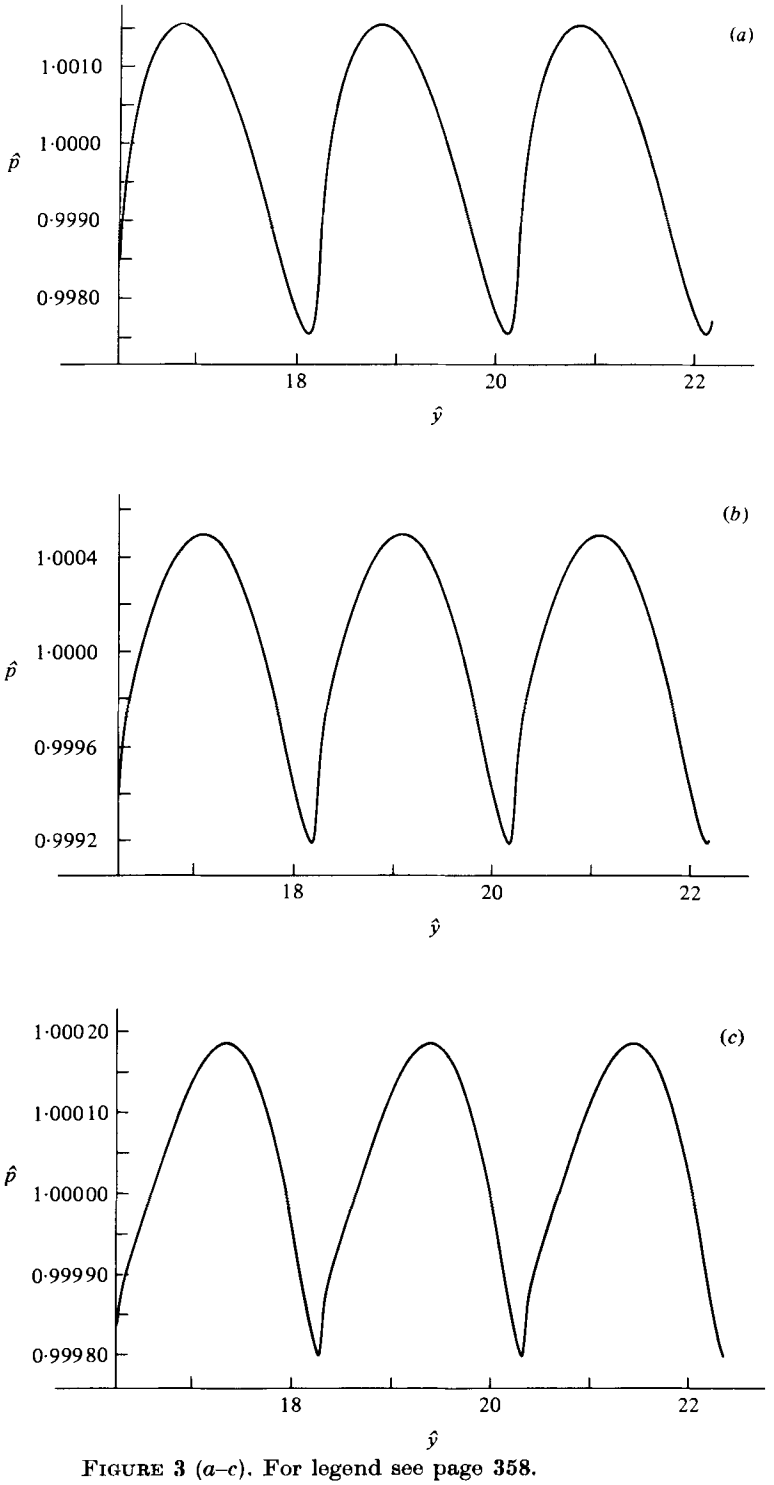

FIGURE 3 (*a–c*). For legend see page 358.

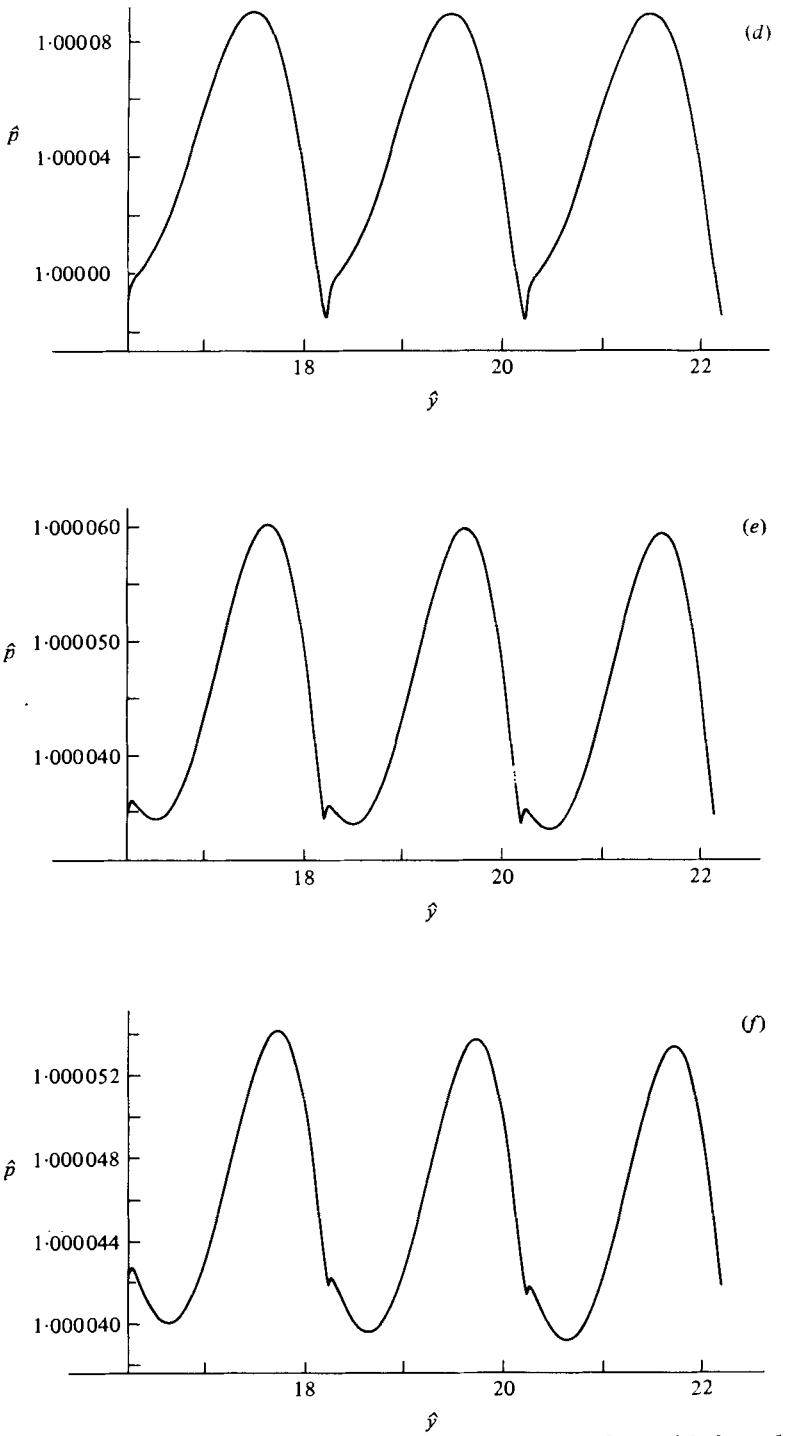

FIGURE 3. Pressure profiles on successive particle paths for a flow with boundary condition equation (58), $\hat{u}_1 = 0{\cdot}015$, $c = 1{\cdot}00$, and $\hat{\omega} = \pi$. The values of $\hat{x}_0$ are (*a*) 53·4, (*b*) 82, (*c*) 112, (*d*) 142, (*e*) 172, and (*f*) 187.

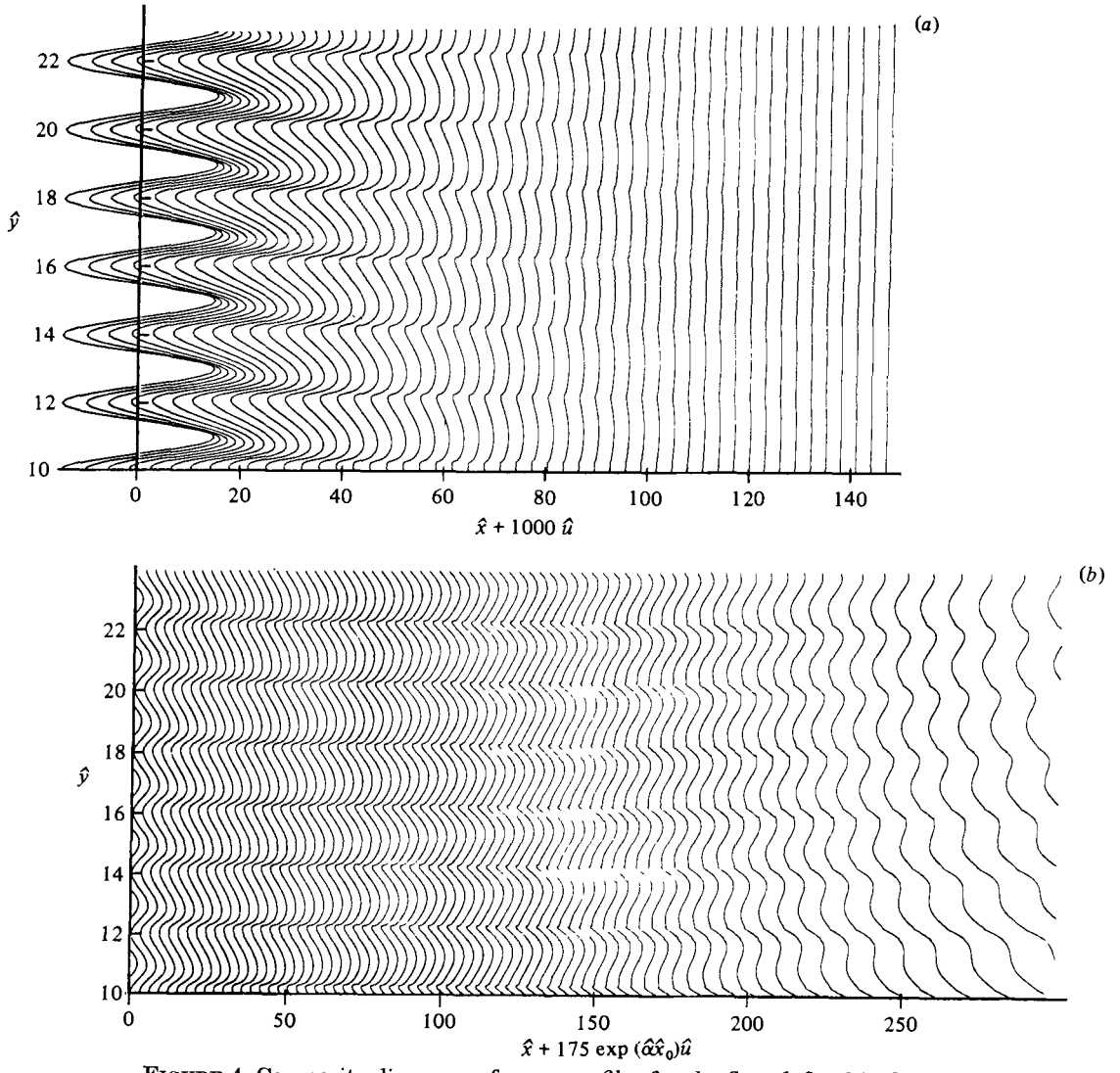

FIGURE 4. Composite diagrams of wave profiles for the flow defined in figure 3: (*a*) profiles of $\hat{u}$; (*b*) profiles of $\exp(\hat{\alpha}\hat{x}_0)\hat{u}$.

diverges from this direction, since its rate of propagation is then close to the frequency-dependent linear sound speed which is smaller than the frozen (high-frequency) a_0. What is more, the kink can be seen to be related to a region of high compression which forms in the wave in the near field. The kink propagates at a rate which is close to a_0 so that this part of the signal then travels on lines parallel to $\hat{Y}$ = constant throughout the far field.

Figure 4 was reproduced directly from the computer graph-plotter output and is therefore not of the same quality as the rest of the figures, which have been traced from the graph-plotter output.

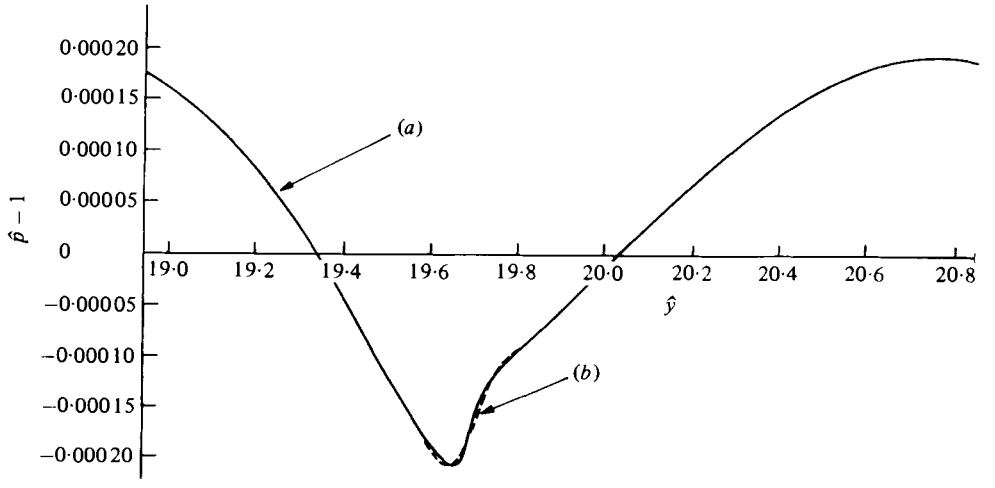

FIGURE 5. The wave profile at $\hat{x} = 111$ for the flow defined in figure 3: (*a*) calculated wave; (*b*) mean and first 13 harmonics.

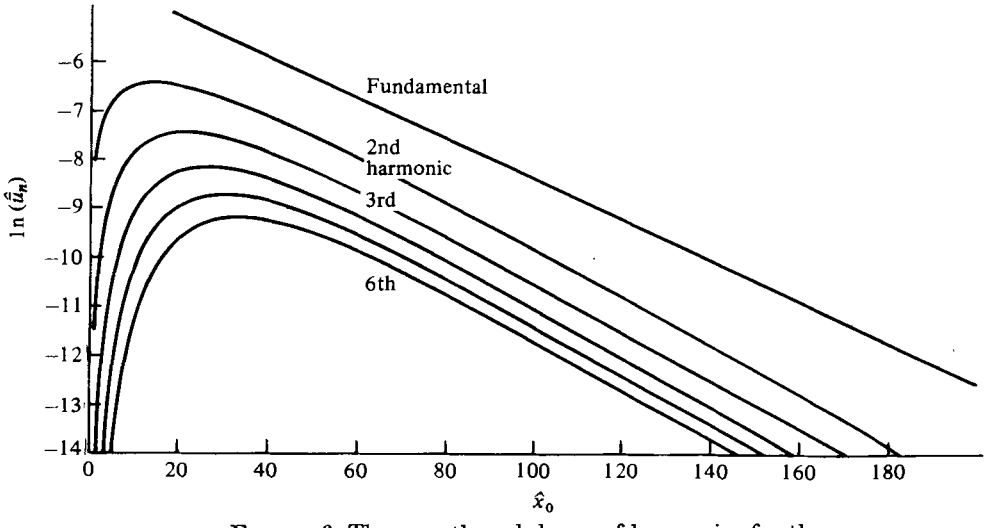

FIGURE 6. The growth and decay of harmonics for the flow defined in figure 3.

8. Fourier analysis and comparison with the Pernet & Payne method

Any periodic waveform can be expressed as a Fourier series. In our case the Fourier coefficients were obtained by a very simple numerical integration process using the trapezium rule. Nevertheless, the method appeared satisfactory and some impression of its effectiveness can be gained from figure 5 which demonstrates that the numerically calculated wave and the wave made up from the first thirteen numerically calculated harmonics are indistinguishable except in the trough.

We can therefore plot the amplitude of each harmonic as a function of x. An example of such a plot is shown in figure 6. It was found that for $\hat{x} > 80$ the harmonics decayed

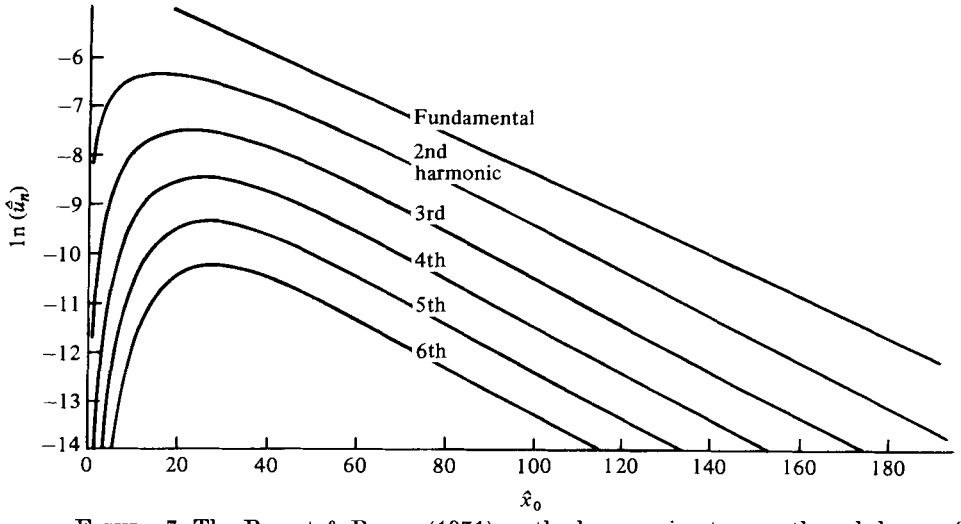

FIGURE 7. The Pernet & Payne (1971) method approximate growth and decay of harmonics for the flow defined in figure 3.

according to linear acoustics and indeed, because of the particular dissipation mechanism involved, the higher harmonics all decay at a rate close to the limit of α as $\omega\tau$ tends to infinity.

Plots such as figure 6 only show the amplitude behaviour of the harmonics and do not give any information about their relative phases. The actual wave form can therefore not always be reconstituted from the information contained in this type of figure. This is a drawback in the Pernet & Payne method, which essentially provides the same type of information, when it is applied to gases with strong dispersion, although this is probably not very serious for air.

Figure 7 is the equivalent to figure 6, but using the Pernet & Payne method. The curves in the two figures have similar overall behaviour but the approximate method gives somewhat smaller maximum amplitude of the higher harmonics than those found from the exact numerical analysis.

A clearer comparison is seen on the composite figure 8 which shows the curves for the first four harmonics from figures 6 and 7 superimposed. Although the differences are noticeable the approximation still gives a good estimate of the behaviour of the calculated wave. The decay of the fundamental in figures 6, 7 and 8 was found to be very close to that predicted by linear acoustics, demonstrating that the feeding of higher harmonics does not significantly affect the total energy in the fundamental.

There is some indication that the interaction between harmonics in the real flow is different from that in the Pernet & Payne model. The difference seems to depend on harmonic number, the best agreement being for the third harmonic. The difference becomes very large for the high harmonics. D. T. Blackstock suggested some years ago in unpublished work and in a recent private communication that a sounder approach than that used by Pernet & Payne would be to express the u_1^n term in the Fubini solution as the correct combination of terms modelling the actual generation of harmonics as described above in § 3. This leads to an explicit expression for the third harmonic, which, however, in our case was found to deviate far more from the numerical

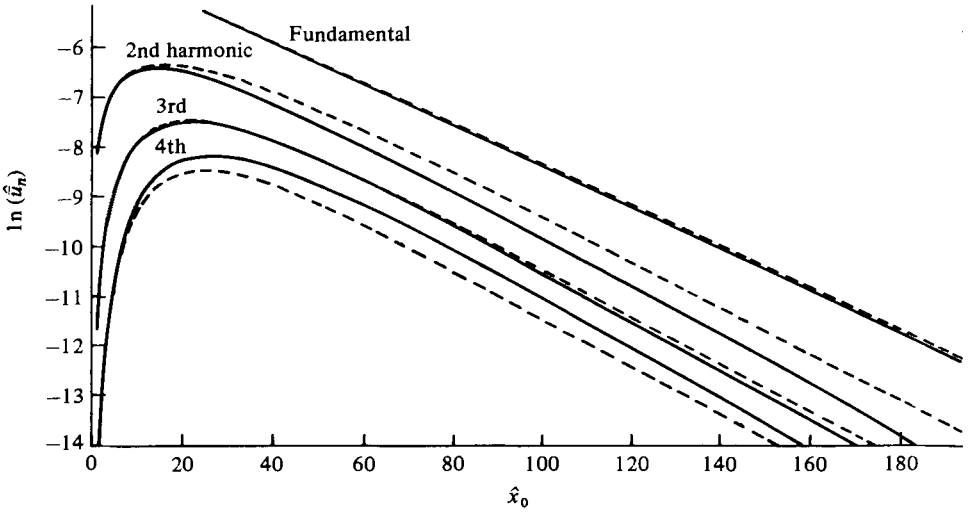

FIGURE 8. Comparison between figures 6 and 7. ——, calculated, — — —, approximate.

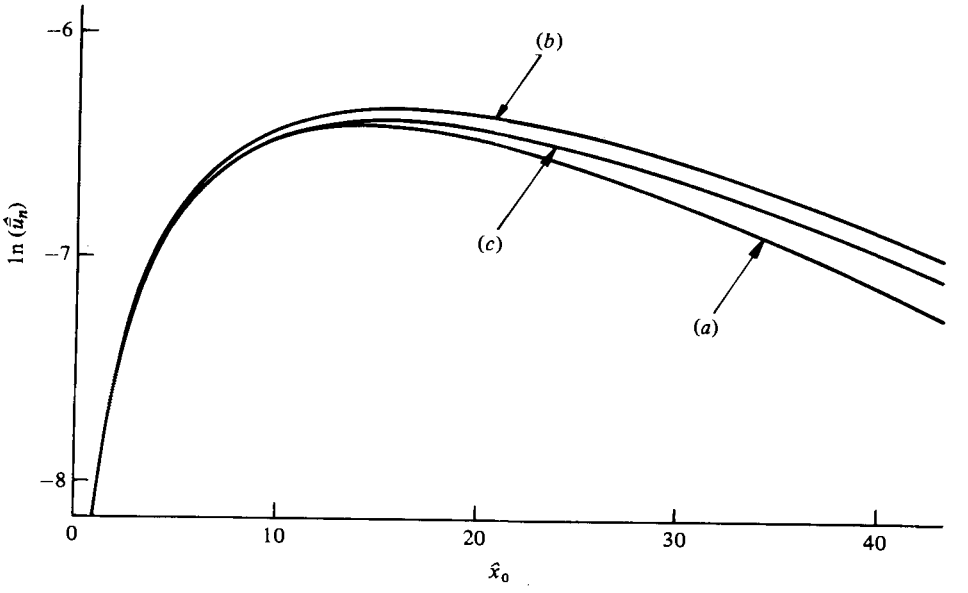

FIGURE 9. Comparison of the developments of the second harmonic in the flow defined in figure 3: (*a*) numerical; (*b*) equation (49); (*c*) equation (52).

solution than did the Pernet & Payne expression. For higher harmonics the Blackstock approach becomes progressively more difficult. It therefore appears that the effects of the various imperfections in the Pernet & Payne approach to some extent cancel out in the first few harmonics.

In §5 we suggested that the Pernet & Payne method might be improved by including higher terms in the series expansion for the Bessel function. Figure 9 demonstrates this by comparing (49) and (52) for the second harmonic. Clearly, using the

improved expression increases the distance over which the approximate and exact curves agree.

9. Conclusions

We have attempted to demonstrate that the accuracy and capacity of computers are now such that it is possible to calculate periodic wave propagation phenomena for distances over which the amplitude decays by several orders of magnitude. Our aim has been to discuss the methods and to illustrate them by selected results rather than to give comprehensive results. This is because we feel that the oscillating piston problem, although interesting, lacks direct practical application. The paper should therefore be looked at as a first step in a move towards more realistic problems. In particular, the extension to the pulsating sphere problem is already under way, and there seems no doubt that it will eventually be possible to treat flows with more complicated boundary conditions in gases with low vibrational specific heats and in mixtures of such gases.

We do not see our approach as an alternative to approximate analytical methods but rather as a means of assessing the accuracy and applicability of such methods. This will hopefully lead to a clearer assessment of the conditions under which nonlinear propagation effects are of practical importance.

We have had many helpful discussions with Dr J. P. Hodgson and Mr W. A. Scott. We are particularly grateful to Dr Hodgson for supplying the original computer program for piston-generated pulse propagation on which our numerical approach was based. I.S.S. was in receipt of a Research Studentship from the Science Research Council.

Appendix

Equation (50) has the following solutions for n equals 2, 3, 4, 5, and 6.

For $n = 2$,

$$\bar{u}_2 = \frac{u_1}{2x_s(2\alpha_1 - \alpha_2)} (\exp[-\alpha_2 x) - \exp(-2\alpha_1 x)].$$

For $n = 3$,

$$\bar{u}_3 = \frac{3u_1}{4x_s^2(3\alpha_1 - \alpha_3)^2} [\exp(-\alpha_3 x) - \exp(-3\alpha_1 x)] - \frac{3u_1}{4x_s^2(3\alpha_1 - \alpha_3)} x \exp(-3\alpha_1 x).$$

For $n = 4$,

$$\bar{u}_4 = \frac{2u_1}{x_s^3(4\alpha_1 - \alpha_4)^3} [\exp(-\alpha_4 x) - \exp(-4\alpha_1 x)]$$

$$- \frac{u_1}{x_s^3(4\alpha_1 - \alpha_4)} \left(x^2 + \frac{2}{4\alpha_1 - \alpha_4} x\right) \exp(-4\alpha_1 x).$$

For $n = 5$,

$$\bar{u}_5 = \frac{125u_1}{16x_s^4(5\alpha_1 - \alpha_5)^4} [\exp(-\alpha_5 x) - \exp(-5\alpha_1 x)]$$

$$- \frac{125u_1}{96x_s^4(5\alpha_1 - \alpha_5)} \left(x^3 + \frac{3x^2}{5\alpha_1 - \alpha_5} + \frac{6x}{(5\alpha_1 - \alpha_5)^2}\right) \exp(-5\alpha_1 x).$$

For $n = 6$,

$$\bar{u}_6 = \frac{3^4 u_1}{2x_s^5(6\alpha_1 - \alpha_6)^5}[\exp(-\alpha_6 x) - \exp(-6\alpha_1 x)]$$

$$-\frac{3^3 u_1}{2^4 x_s^5(6\alpha_1 - \alpha_6)}\left(x^4 + \frac{4x^3}{(6\alpha_1 - \alpha_6)} + \frac{12x^2}{(6\alpha_1 - \alpha_6)^2} + \frac{24x}{(6\alpha_1 - \alpha_6)^3}\right)\exp(-6\alpha_1 x).$$

REFERENCES

BLACKSTOCK, D. T. 1962 Propagation of plane sound waves of finite amplitude in non-dissipative fluids. *J. Acoust. Soc. Am.* **34**, 9–30.

BLACKSTOCK, D. T. 1964 Thermoviscous attenuation of plane, periodic, finite amplitude sound waves. *J. Acous. Soc. Am.* **36**, 535–542.

BLYTHE, P. A. 1969 Non-linear wave propagation in a relaxing gas. *J. Fluid Mech.* **37**, 31–50.

DAIN, C. G. & HODGSON, J. P. 1975 The development of weak waves in the unsteady one-dimensional flow of a vibrationally relaxing gas ahead of an impulsively started piston. *J. Fluid Mech.* **69**, 129–144.

HERZFELD, K. F. & LITOVITZ, T. A. 1959 *Absorption and Dispersion of Ultrasonic Waves.* Academic Press.

HODGSON, J. P. & JOHANNESEN, N. H. 1976 'The effects of vibrational relaxation on the development of weak nonlinear waves in air. *Proc. 6th Int. Symp. on Nonlinear Acoustics*, vol. 1, pp. 30–40. Moscow State University.

HORNBY, R. P. & JOHANNESEN, N. H. 1975 The development of weak waves in the steady two-dimensional flow of a gas with vibrational relaxation past a thin wedge. *J. Fluid Mech.* **69**, 109–128.

JOHANNESEN, N. H. & HODGSON, J. P. 1979 The physics of weak waves in gases. *Rep. Progress Phys.* **42**, 629–676.

JOHANNESEN, N. H. & SCOTT, W. A. 1978 Shock formation distance in real air. *J. Sound Vib.* **61**, 169–177.

KAO, J. & HODGSON, J. P. 1978 Supersonic flow of a vibrationally relaxing gas past a circular cone. *J. Fluid Mech.* **85**, 519–542.

LIGHTHILL, M. J. 1956 Viscosity effects in sound waves of finite amplitude. In *Surveys in Mechanics* (ed. G. K. Batchelor & R. M. Davies), pp. 250–351. Cambridge University Press.

PERNET, D. F. & PAYNE, R. C. 1971 Non-linear propagation of signals in air. *J. Sound Vib.* **17**, 383–396.

RUDENKO, O. V. & SOLUYAN, S. I. 1977 Theoretical foundations of nonlinear acoustics. Plenum.

WEBSTER, D. A. & BLACKSTOCK, D. T. 1978 Experimental investigation of outdoor propagation of finite-amplitude noise. *N.A.S.A.* CR-2992.